CRACK PROPAGATION UNDER WATER PRESSURE

REPORT 2018:487





Crack Propagation under Water Pressure

Experimental and Computed Tomography Investigation

LAMIS AHMED
ALVARO GUARIN
ALI NEJAD GHAFARS

Foreword

The stresses induced by water pressure inside a crack or interface between two materials can be a decisive factor for extension of the crack and/or triggering a failure process. Therefore, knowledge about the water pressure inside the cracks and interfaces is important for a safer design of hydraulic structures.

The stress level and distribution along with the crack or interface may determine the structural safety and stability, and they are both governed by the crack's width or the distance between two faces of the interface. Both parameters are governed by the displacement and rate of the displacement of the structure. Due to the mentioned factors the uplift pressure (stress) in the same concrete gravity dam may show three different level and distribution during static (permanent loading), quasi static (seasonal variations) and earthquake (dynamic) conditions.

This study was led by Dr Lamis Ahmed, assistant principal at the Royal Institute of Technology in Stockholm. It was performed within Energiforsk Concrete R&D program hydropower. The program is financed by Fortum Sverige AB, Jämtkraft AB, Karlstads Energi AB, Skellefteå Kraft AB, Sollefteåforsens AB, Statkraft Sverige AB, Svensk Kärnbränslehantering, Sydkraft Hydropower AB, Umeå Energi AB, Vattenfall AB Vattenkraft och Vattenfall Indalsälven AB.

Reported here are the results and conclusions from a project in a research program run by Energiforsk. The author / authors are responsible for the content and publication which does not mean that Energiforsk has taken a position.



Sammanfattning

Sprickor i betongkonstruktioner, såsom betongdammar, kan utsättas för vattentryck, t.ex., upplyftningstryck. Vattentrycket kan vara signifikant och kan resultera i sprickor som propagerar genom konstrukturerna och därför kan resultera i minskad livslängd. Kunskapen om vattentrycket inom sprickorna är emellertid relativt begränsad och försummas ofta eller uppskattas mycket approximativt. Inverkan av spricköppningshastigheten på upplyftningstrycksfördelningen i sprickan och tryckvariationen under öppning eller plötslig sprickförslutning är frågor som behöver undersökas.

Som ett försök att svara på dessa frågor beskrivs här en pilotstudie som visat möjligheterna och begränsningarna för den föreslagna experimentella uppställningen och tekniken (penetrabilitetsmätare och tomografi) som en undersökningsmetod för vattentryck i betongssprickor. De provkroppar som undersöks här är uteslutande cylindrar gjutna av betong med eller utan en första spricka.

Penetrabilitetsmätaren kan användas för att applicera vattentryck och för att visualisera spricköppningen. Försök med röntgen och datatomografi utfördes på KTH, institutionen för byggvetenskap.

Exemplen som rapporteras i detta arbete visar att tekniken och utrustningen har stor potential för framtida arbete med att analysera sprickbildning, men försöksuppställningen inklusive förberedelse och utförande behöver ytterligare utveckling.



Summary

Cracks in concrete structures such as a concrete dam can be exposed to water pressure, for example, uplift pressure. The water pressure can be significant and may result in cracks propagating through the structures and thus it may result in reduced service life. However, the knowledge of water pressure within the cracks is relatively limited and is often neglected or just roughly estimated. The influence of crack opening rate on the uplift pressure distribution in the crack and the pressure variation during opening or sudden crack closure are questions needed to investigate.

As an attempt to answer those questions, a pilot study presented here describes the possibilities and limitations of the proposed experimental setup; and technology (penetrability meter and tomography) as an examination method for water pressure in propagation concrete cracks. The test specimens examined here are exclusively cylinders cast of concrete with or without an initial crack.

The penetrability meter can be used to apply water pressure and to visualize the crack opening, X-Ray computed tomography test, was performed. KTH Civil and Architectural Engineering department has organized the laboratory resources.

The examples reported in this work show that the technology and equipment have great potential for future work on crack propagation, however, sample design and preparation, as well as testing need further development.



List of content

1	Intro	duction		8
	1.1	backg	round	8
	1.2	Aim		9
	1.3	Objec	tives	9
	1.4	limita	tions	9
2	Instr	umentat	ions	10
	2.1	Penet	rability meter	10
	2.2	Tomo	graphy	11
3	Simu	lation of	f crack propagation	16
	3.1	Types	of crack	16
	3.2	Crack	propagation	17
		3.2.1	Tensile behaviour of concrete	17
		3.2.2	Fracture mechanics	18
	3.3	Fluid i	n cracks	20
		3.3.1	Fluid flow through cracks	20
		3.3.2	Fluid pressure in cracks	20
	3.4	Finite	Element Method	21
		3.4.1	Model geometry	22
		3.4.2	Material properties	22
		3.4.3	Interface and boundary conditions	23
		3.4.4	EF results	24
	3.5	Conclu	usions	25
4	Inves	tigation	method	26
	4.1	Concrete mix		
	4.2	Fabric	ration of test specimens	27
		4.2.1	First attempt	27
		4.2.2	Second attempt	29
	4.3	Experi	imental procedure	32
		4.3.1	Applying water pressure	32
		4.3.2	CT scan	33
5	Resu	Its and d	liscussion	34
	5.1	Water	pressure time history	34
		5.1.1	First attempt	34
		5.1.2	Second attempt	35
	5.2	Tomo	graphy visualization	37
		5.2.1	Visualization of water in concrete sample	37
		5.2.2	Visualization of cracks in concrete induced by pressurized water	38
	5.3	Discus	ssion	41



6	6 Conclusions and further research		
	6.1	Conclusions	42
	6.2	Recommendations	42
Refere	ences		44



1 Introduction

1.1 BACKGROUND

Propagating cracks in concrete dams occur mainly in earthquakes and temperature changes. Crack growth may also occur for other reasons, due to mechanical loads exceeding the load capacity, e.g. ice pressure. Historical evidence (Hansen and Roehm, 1979) has shown that gravity and buttress dams subjected to strong earthquake ground motions are likely to develop cracks in the upper dam section and near the dam–foundation interface, see Figure 1.1. Uplift pressures acting along cracks and joints create external forces that favour crack propagation in the dam body and affect the dynamic and post-seismic stability of cracked concrete components. Slowik and Saouma (2000) reported experimental results related to water pressurization of propagating cracks in concrete specimens in a dynamic wedge splitting test. It was observed that the crack opening rate could have an important consequence on the internal water pressure magnitude and distribution. If the crack opening rate is slow enough, the water pressure has time to develop, whereas under fast crack openings the waterfront cannot keep up with the crack front.

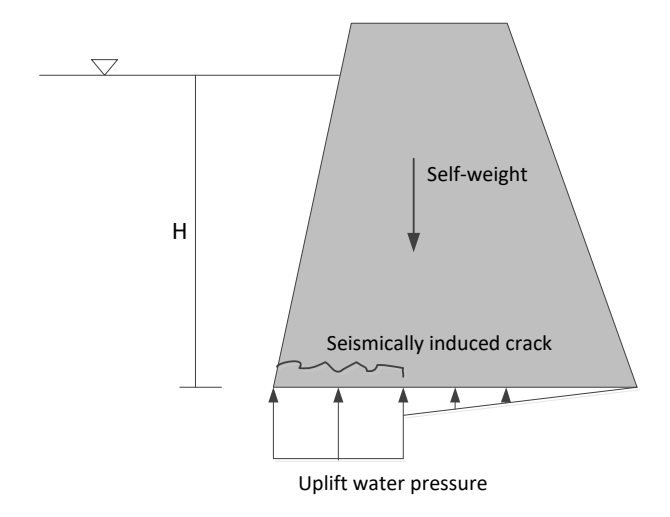


Figure 1.1: Full uplift pressure is attained instantly in seismic cracks, according to (Farrokh, Pierre and René, 2005)

However, there is limited knowledge about the influence of crack opening rate on the uplift pressure distribution in the crack and what is the pressure variation during opening or sudden crack closure. To answer this question, a pilot study presented here describes the possibilities and limitations of experiment and technology as an examination method for water pressure in propagation concrete cracks. If the technique as such proves to be useful to evaluate the water pressure distribution along the crack, the benefit will be great. The test bodies examined here are exclusively cylinders cast of concrete with or without an initial crack. For



more visualization of the crack opening a tomography test is also performed. KTH Civil and Architectural Engineering department have organized the laboratory resources, and these now include an advanced system for tomography of material samples. The equipment is integrated with a computerized visualization system and has also an MTS equipment for tensile and pressure testing as well as a climate chamber operating within the temperature range -20°C to + 80°C. The equipment was originally procured for studying asphalt samples but is also suitable for generating three-dimensional screening images of, for example, concrete. The experience of using the equipment to test such materials was previously small and there were neither any instructions on how it could be done nor where the limits of usability were. Therefore, this laboratory pilot study was conducted to provide a description of the possibilities and limitations of the technology as well as the use of work and routines for examination.

1.2 AIM

The pilot study aims at investigating how to design an experimental model to evaluate the crack propagation behaviour under the influence of water pressure and how tomography can be used to visualize the crack propagation. The aim is to get a description of the possibilities and constraints of this combined technology areas as well as the workflow, and thus indirect working time, to use the method of calculating fracture opening along the crack path suitably.

1.3 OBJECTIVES

The main objectives of this project are:

- Is it possible to observe differences in water saturated and dry concrete, using tomography?
- How can an experimental specimen be designed to be rotationally symmetrical (a requirement for scanning around the test specimens)?
- Design of the test setup in order to carry out the pressure test of the concrete specimen.
- Evaluate the use of X-Ray computed tomography CT for crack detection in a water-induced crack in the concrete.

1.4 LIMITATIONS

Within the budget available for this project, several key components of the project had to be prioritized including design and implementation of the experimental setup, mainly the system to apply the pressurized water. In addition, crack initiation mechanism inside the concrete specimens. These were highly time-consuming items within the project.

The potential of X-Ray computed tomography CT had also been slightly constrained; for example both water and cracks detection in concrete would need more time available for better data acquisition and data analysis/algorithms. Furthermore, the use of the CT equipment is time-consuming.



2 Instrumentations

This section presents the instrumentation devices used for the experimental test. To give the reader a good understanding, a description of each device's specification, position and purpose are presented.

2.1 PENETRABILITY METER

The modified penetrability meter consists of a grout container connected to an outlet pipe with a valve and a filter unit to hold the filter. The filters fitted in the cup holder are woven metal wire cloths with different mesh sizes of 26-200 μ m. The applied pressure is supplied by a gas container with 300 bars capacity and the pressure is controlled by a pressure regulator. The instrument is connected to a load cell (S9M) that registers weight changes and send the data to a computer via a data acquisition system (QuantumX MX471B). The weight in time graph is plotted using Catman program. Any pressure changes are also registered by a pressure transducer. See the details of the system's outline in Figure 2.1.

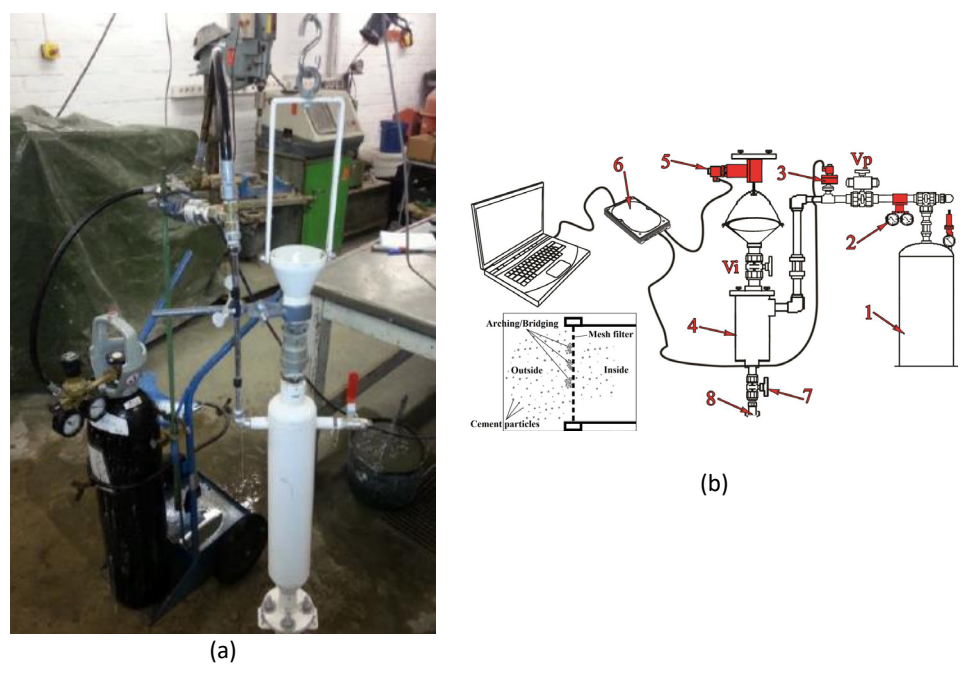


Figure 2.1: Penetrability meter: (a) photo of the penetrability meter, (b) schematic depiction of modified penetrability meter and details of arching/ bridging at mesh filter, (1) gas tank, (2) pressure regulator, (3) pressure sensor, (4) grout tank, (5) load cell, (6) DAQ-data acquisition system, (7) outlet valve, (8) filter holder (Nejad Ghafar, 2017).

For practical reasons, the experiments are performed with 20 bar pressure only which is equal to 2 MPa. Therefore, low strength concrete is used in this experiment to produce an initial crack exceeding the material's failure strength i.e. the tensile strength of concrete.



The pressure-time measurement starts by opening the outlet valve and beginning the water flow when a sharp peak in pressure occurs until the gas inflow compensates the water discharge at the balance point. The pressure then remains constant. Testing at different interval time pressures will give a better understanding of the crack propagation behaviour inside the concrete specimens.

2.2 TOMOGRAPHY

X-ray computed tomography (CT) is a non-destructive technique used for visualizing the interior of solid objects using digital information of the objects down to microscopic detail level. Medical CT systems are used for acquiring an image of soft tissues and bones while high-resolution industrial X-ray CT utilizes higher energy X-rays with more penetrative power and is used for materials within disciplines such as geosciences, engineering and manufacturing.

A cylindrical volume can be described by sequential 2D CT images, corresponding to slices with an associated thickness that together defines the volume as composed of 3D elements, i.e. voxels. The quality of these scanned images depends on the Xray source, the detectors used and the scanning configuration. More details on the sequential procedure of sample preparation, calibration, data acquisition and reconstruction are given by e.g. Ketcham and Carlson (2001). The X-ray CT system used in this study is of the type NSI X5000 (North Star Imaging Ins, 2016), see Figure 2.2 - 2.3. Within a radiation shielded enclosure, there are 225 kV and 450 kV X-ray tubes with focal spot sizes of 5 µm and 400 µm, respectively, with a highresolution digital detector with 200 µm pixel pitch, see Figure 2.4. Depending on specimen size, the degree of geometrical magnification and the tube used, tomography data with voxel sizes down to 5 μm can be obtained. The system also contains a workstation with software for CT calibration, cone-beam reconstruction, 3D real-time visualization and numerical analysis tools. There is also an integrated MTS Model 370 Uniaxial Test System for up to 100 kN force and 150 mm displacement, see Figure 2.5 and a chamber that can produce testing temperatures within -20°C to +80°C, see Figure 2.6.



Figure 2.2: NSI X5000 system at KTH Civil and Architectural Engineering department.





 $Figure\ 2.3:\ Digital\ detector\ with\ 200\ mm\ pixel\ pitch\ in\ the\ NSI\ X5000\ system.$



Figure 2.4: X-ray sources with 225 kV and 450 kV in the NSI X5000 system.



Figure 2.5: Mechanical MTS 810 in NSI X5000 system load system.



Figure 2.6: Climate chamber connected to the NSI X5000 system.

The computer imaging equipment used in this project has previously been used to investigate samples of steel fibre reinforced shotcrete (sprayed concrete), see Ansell, Ahmed and Guarin (2017). A laboratory study has been conducted to examine how CT can be used as a laboratory method for investigation of cored specimens of shotcrete from tunnels. The method was well suited to describe the distribution and orientation of steel fibres in the shotcrete, and also how interfaces between rock-shotcrete and between layers of different spray stages can be detected. In addition, in order to obtain information on cracked steel fibre concrete, the splitting tensile test for one cylinder concrete specimen was carried out. From the obtained CT images of the specimen that were converted to three-dimensional images, a visualisation of the specimens can be obtained as shown in Figure 2.7-2.9. In Figure 2.7, a photo and a three-dimensional CT image of the specimen exterior and a 3D



image showing the steel fibre configuration only, which shows that the fibre orientation is highly variable. The second example in Figure 2.8 shows the visualisation of the cracked specimen. The specimen after failure shows a small broken area near the point of load application. The crack paths through the specimen are shown in Figure 2.8 a. In the enlarged frame of Figure 2.9, it is clear that the crack, with a width of 0.607mm, is barely noticeable due to the higher density of steel fibre surrounding the crack. It demonstrates that the area of low fibre density at the top and bottom of the image was far more susceptible to cracking than the high fibre density area at the middle part. However, the fibre distribution has a significant impact on the structure of cracks. In addition, the presence of fibres increased the tensile strength of conventional reinforced concrete.

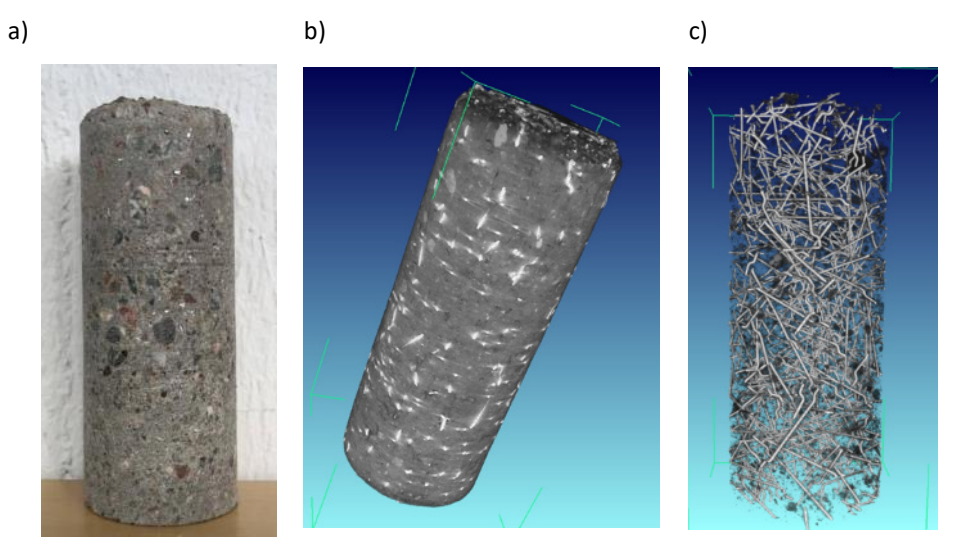


Figure 2.7: Shotcrete core drilled out from a laboratory test beam (a) photo of the sample, (b) CT image of its outer cylinder surface and (c) of the steel fibre configuration only (Ansell, Ahmed and Guarin, 2017).

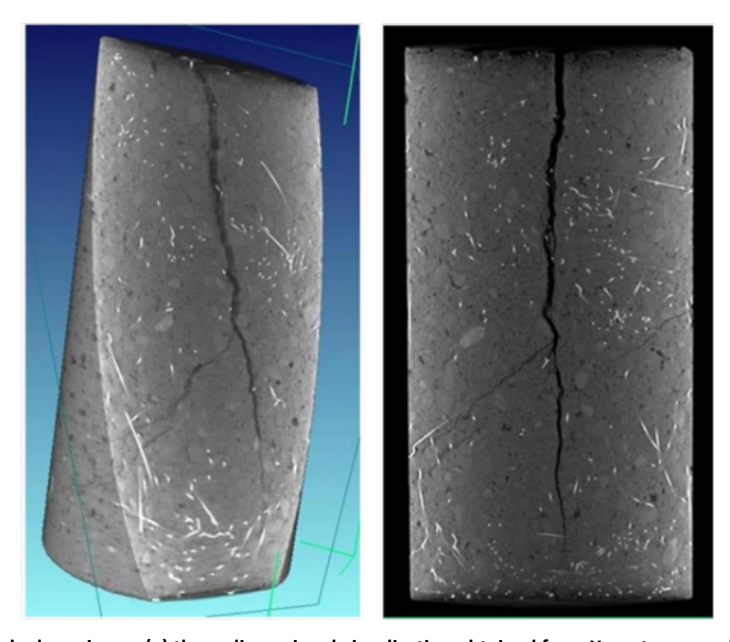


Figure 2.8: Cracked specimens (a) three-dimensional visualisation obtained from X-ray tomography (b) two dimensional CT image.



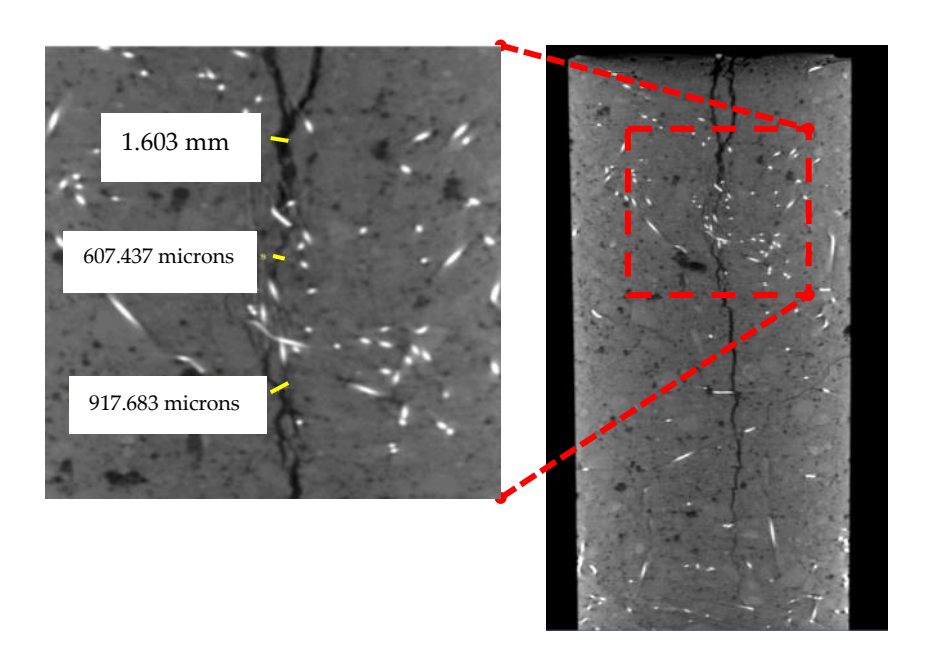


Figure 2.9: The density distribution of steel fibre cracked concrete.



3 Simulation of crack propagation

The effects of cracks in concrete dams are significant and can eventually reduce the bearing capacity and lifetime of the concrete structure. Cracking can cause deflection and deformation of the dam, i.e. movements and shape changes of the structure. This chapter summarizes a simulation study that was performed by Sohrabi and Sanchez Loarte (2017) at KTH Royal Institute for Technology to study crack propagation influenced by water pressure and also to define an experimental test setup that allows for crack propagation due to water pressure. Numerical analyses have been performed on an initially cracked specimen to study the pressure along the crack propagation. The finite element (FE) method has been used as the numerical analysis tool, through the use of the software Abaqus.

At first, the types of crack, crack propagation and fluid in the crack are summarized and some of the practical aspects to be implemented in finite element modelling are given. Then follows a section that briefly describes numerical models based on FE method that has been used to simulate crack propagation under water pressure loads. The experimental setup will be defined in Chapter 4.

3.1 TYPES OF CRACK

Cracking occurs whenever the tensile strain to which concrete is subjected exceeds the tensile strain capacity of concrete. Cracks in concrete occur in different stages and can be divided into two categories; Pre-hardening cracks and post-hardening cracks. Table 3.1 summarizes various possible causes of cracking (*Durable Concrete Structures: Design Guide*, 1992).

Table 3.1 Types of crack based on (Durable Concrete Structures: Design Guide, 1992)

Types of crack		Causes	
		Shrinkable aggregate	
	Physical	Drying shrinkage	
		Crazing	
		Corrosion of reinforcement	
	Chemical	Alkali-aggregate reactions	
		Cement carbonation	
act hardoning		Freeze/thaw cycles	
ost- hardening	Thermal	External seasonal temperature variations	
		Early thermal contraction	
		-External restraint	
		-Internal temperature gradients	
	Structural	Accidental overload	
		Creep	
		Design Loads	
		Early frost damage	
	Plastic	Plastic shrinkage	
re-hardening	FIdSUC	Plastic settlement	
	Constructional	Formwork movement	
	movement	Sub-grade movement	



There are three major cracking causes to consider in the dam; temperature variation, chemical reaction and load. In a dam, loads could be caused by settlement or sliding off the foundation or abutments, ice, salt, waves, earthquakes, or even bombs. It can also cause the offset, i.e. one side of the cracked dam moves with respect to the other side of the dam. It can occur at the edge of a crack or inside a crack and consequently cause horizontal or vertical movements.

Another predominant effect of cracking is efflorescence which appears as a white substance on the surface of the dam; this phenomenon is caused by a chemical reaction within the concrete and transmits to the surface by moisture, see Figure 3.1.



Figure 3.1: Efflorescence stains at the concrete surface due to cracking.

3.2 CRACK PROPAGATION

Crack initiation is a process of separation in the previously un-cracked material. Extending or growing of this initial crack due to exceeding of the material's failure strength is called crack propagation. Since the concrete behaviour is dominated by tensile cracking, propagation of cracks in materials is described within the field of Fracture Mechanics.

3.2.1 Tensile behaviour of concrete

The tensile behaviour of the porous concrete material is brittle. Tensile failure is initiated by micro-cracks with increasing size and number and finally merging creating an actual crack. Micro-cracks are the response of local damage in the material and are initiated in the weakened zones where the stress concentrations are high e.g. between aggregates and cement paste (Björnström, Ekström and Hassanzadeh, 2006). The material response of a specimen subjected to uniaxial tensional load is initially linear elastic up to the level just before reaching the tensile strength f_t . When the applied load increases above this level i.e. at the level of $\sigma = f_t$ the specimen reaches failure and is divided into two separate parts, see Figure 3.2. Before reaching the tensile strength, the extent of micro-cracks is small and distributed over the entire volume. Crack growth will stop if the load is maintained at this level. If the load increases above this level, crack propagation becomes unstable i.e. uncontrolled propagation due to the amount of strain energy released to make the crack propagate by itself. At the maximum level of stress, micro-cracks propagate and are concentrated in a limited area, called the fracture process zone. All micro-cracking will happen within this area and the increased



deformation will lead to merging of the micro-cracks. This behaviour can be seen in Figure 3.1 where the stress-strain curve descends and the material is softening. When micro-cracks are finally merged, a macrocrack is created and visible. Macrocracks are defined as traction free and visible; this step is the resulting stage in which the specimen is separated(Malm, 2016).

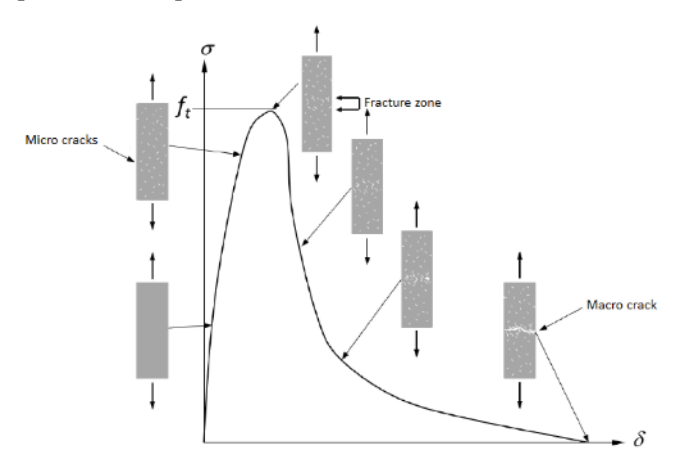


Figure 3.2: Formation of micro-cracks for a specimen under uniaxial tensile loading and the formation of the macrocrack within the fracture process zone, reconstructed from (Hassanzadeh and Westberg, 2016)

3.2.2 Fracture mechanics

Fracture mechanics describes the non-linear behaviour of the crack opening in concrete. The non-linear behaviour can be described as three different failure modes, see Figure 3.3. Mode1 is a normal-opening mode in which concrete is subjected to tension. Mode 2 is caused by shear and mode 3 by a tear. In concrete, mode 1 is the common type of failure which occurs in its pure form. The different failure modes can occur independently or in combination. Mode 2 can be initiated as mode1, i.e. as a crack subjected to tensile stress (Björnström, Ekström and Hassanzadeh, 2006).

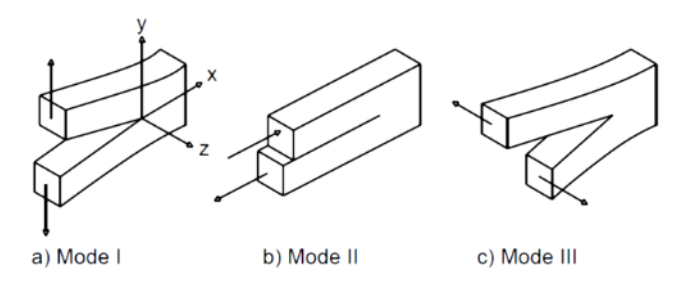


Figure 3.3: Different types of failure modes, (Björnström, Ekström and Hassanzadeh, 2006).

Figure 3.4 illustrates the stress distribution along the fracture zone according to fracture mode 1. The crack is propagated by a macrocrack with an initial length a_0 . Microcracks are successively formed along the fracture process zone l_p . The width of the crack opening is denoted w and w_c is the width of the macrocrack. The stress at the transition zone between macrocrack and fracture zone process is equal to zero. The stress increases in the fracture zone process reaching the maximum value equal to the tensile strength at the crack-tip.



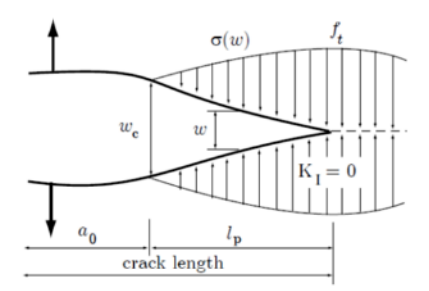


Figure 3.4: Illustration of stress distribution at crack tip according to fracture mode 1, reproduction from (Hillerborg, Modéer and Petersson, 1976)

In order to estimate the uniaxial tensile strength of concrete, the fracture energy and shape of the unloading curve must be established. This information is not available in the Eurocode but can be determined using the Model code (2010). These codes are based on experimental results and the expression used to estimate the fracture energy G_f in mode 1 is given as:

$$G_f = 73 \cdot f_{cm}^{0.18} \tag{1}$$

where,

 f_{cm} is the mean compressive strength of concrete [MPa].

The fracture energy is considered to be a material property of the concrete material in which the crack opening displacement is dependable. This is defined as the amount of energy needed in order to obtain a stress-free tensile crack of unit area, in which it can be illustrated in Figure 3.5. The area under the tensile behaviour curve is denoted G_f and varies along the fracture zone to the crack-tip (Malm, 2016).

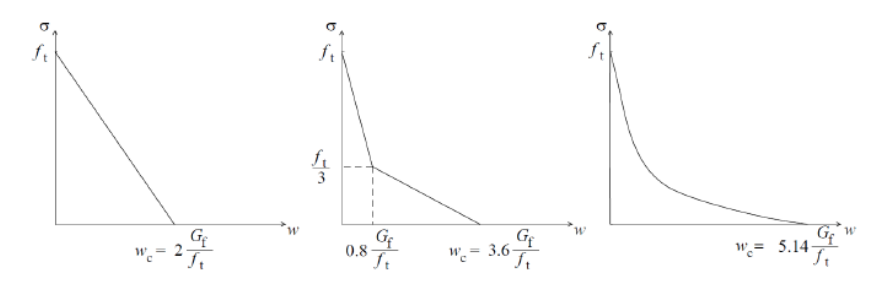


Figure 3.5: Crack opening curves used for numerical analyses. Left to right, Linear, bilinear and exponential, from (Malm, 2016).

The exponential curve can be calculated by the following equation:

$$\sigma = f_t \exp\left(-\frac{f_t}{G_f}COD\right) \tag{2}$$

where, f_t is the tensile strength [Pa], G_f is the fracture energy [Nm/m²] and COD is the crack opening width [mm]



3.3 FLUID IN CRACKS

Fluid driven crack propagation is a process of extending of an existing crack subjected to fluid pressure. Concrete structures such as gravity dams interact constantly with high-pressure water. Existing cracks are filled with a large amount of water which penetrates deeper into the dam and consequently reducing the bearing capacity and safety of the dam (Sha and Zhang, 2017).

There are several earlier studies of fluid-driven crack propagation in concrete structures. Bruhwiler and Saouma (1995) studied water pressure distributions in cracks. It has been shown that the hydrostatic pressure inside a crack is a function of crack opening displacement given the stress continuity in the fracture process zone. This internal uplift pressure reduces full hydrostatic pressure to zero along the fracture process zone. The hydrostatic pressure distribution inside a crack with respect to time and the crack opening rate was examined. It was concluded that the crack opening rate plays an important role in controlling the internal water pressure distribution. Slow crack opening rates give time to the water to flow into and propagate within the crack. The water behaves differently under fast crack opening rates and takes a longer time to develop.

3.3.1 Fluid flow through cracks

Crack propagations can be either static or dynamic. Static crack propagation is when the loading rate is low, i.e. no fluid flow. Higher loading rates correspond to dynamic propagation, i.e. the fluid actually flows in the crack. The flow can behave in a laminar or turbulent manner and depends comprehensively on the crack geometry. The fluid flow in the crack gives rise to a successively dropping pressure along the distance from the crack opening. Besides the type of flow, the pressure drop depends also on the fluid properties. The pressure drop is largest for high viscous fluids due to large friction losses along the crack boundaries (Rossmanith, 1993)

3.3.2 Fluid pressure in cracks

The hydrostatic pressure acting on concrete dams ρgh varies with depth h on the vertical face. The loads that drive crack propagations are only the vertical tensile or compressive stress σ_y and the water pressure P_w inside the crack, see Figure 3.6 (Wang and Jia, 2017)

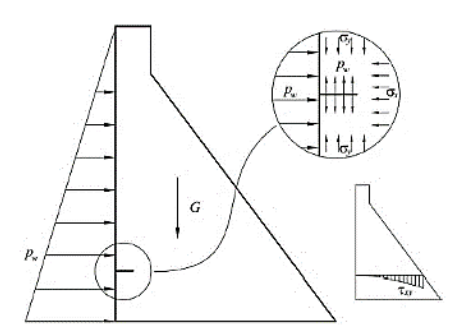


Figure 3.6: Stress condition around the crack in a gravity dam, from Wang and Jia (2017)



Load distributions in concrete dam cracks can be investigated with two boreholes and a fracture linking them, see Figure 3.7. Figure 3.7a illustrates a concrete dam with a crack that has propagated far enough to reach the air on the downstream side. The fluid pressure will be distributed linearly in such a case. The pressure distribution will be even if the crack is completely sealed, see Figure 3.7b and can be expressed as, $P=pgh_1$, where h_1 represents the upstream height. However, this behaviour is not realistic since concrete is a porous material and the water will thus spread out at the crack tip as in Figure 3.7d. Then, the pressure at the crack tip can in such a case be calculated as $P=pgh_2$ where h_2 is the downstream level.

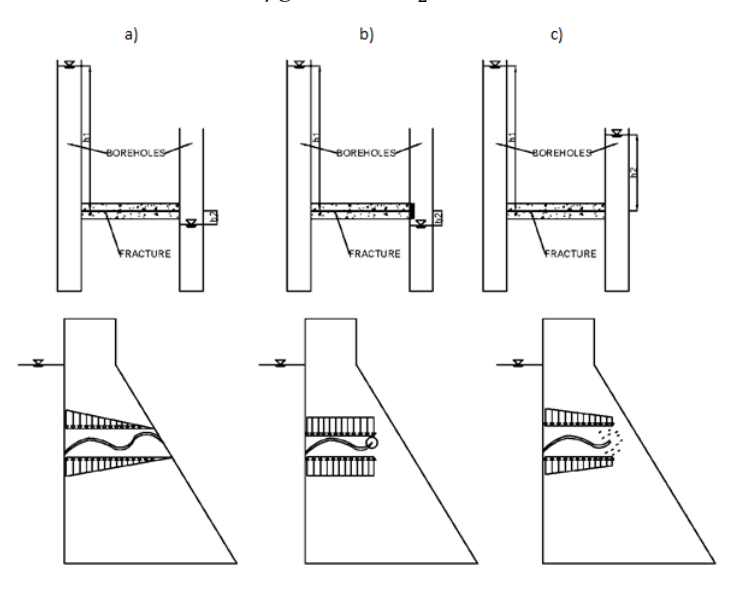


Figure 3.7: Fluid pressure distributions in a) crack in contact with air b) completely sealed crack c) realistic closed crack(Sohrabi and Sanchez Loarte, 2017)

3.4 FINITE ELEMENT METHOD

As mentioned previously, an attempt to investigate how crack propagation behaves under the influence of water pressure, FE models were developed by Sohrabi and Sanchez Loarte (2017) using Abaqus software (Dassault Systémes, 2014). The FE models were introduced here that adapted to represent the experimental specimen. The experimental test was also performed by Sohrabi and Sanchez Loarte (2017) as a first attempt to develop an experimental setup to evaluate the crack propagation influenced by water pressure in concrete cracks. The test set up and results of the experiment will be given in Chapter 4 and 5, respectively. A summary of FE model is described here and for more details, see Sohrabi and Sanchez Loarte (2017).

To determine the critical pressure loads that cause a crack to propagate, linear elastic material properties were used in the simulations. This was performed with the contour integral method where the stress intensity factors were calculated according to linear elastic fracture mechanics. These critical pressure magnitudes were then used as input values to study the pressure distribution along the crack propagation. This was simulated with the cohesive surface-to-surface contact interaction based on non-linear material properties.



Two cases have been analyzed when simulating the critical pressure loads; case a) pressure acting only at the initial crack surface and case b) pressure acting along the crack propagation. The specimens used in this study were of small dimensions and the calculations were performed under highly controlled conditions, which may differ significantly from concrete dams. Case a) can be approximated by the influence of dynamic forces causing sudden crack propagation, such as earthquakes. Water pressure requires time to develop inside cracks in order to reach steady state conditions. In this case of sudden cracks induced by dynamic forces, water pressure may not be able to develop along the propagation. In case b), water pressure has been fully able to develop a wet surface.

3.4.1 Model geometry

The geometry of the FE models is shown in Figure 3.8. As it can be seen in Figure 3.8, an initial crack of length 10 mm and width 0.5 mm has been included in horizontal and vertical directions in model 1 and 2, respectively. The geometry was decided in accordance with the experiment dimensions. The initial crack opening was set to 0.5 mm and has a triangular shape.

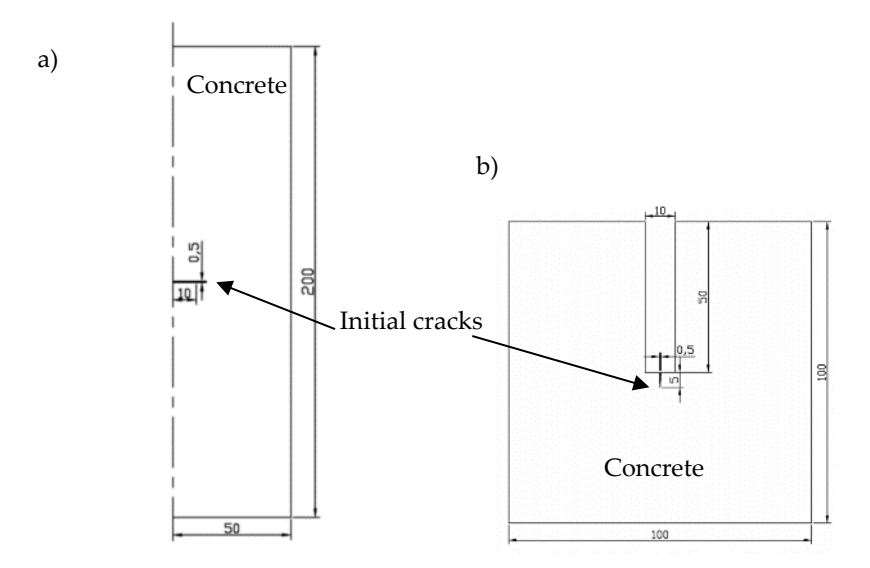


Figure 3.8: Configuration of FE models (a) axisymmetric model 1 and(b) model 2. All dimensions are in mm.

3.4.2 Material properties

The material properties used in the FE analysis are presented in Table 3.2. Properties for the concrete are assumed to be of quality C20/25 according to (Eurocode 2, 2011). In this study, the concrete behaviour is dominated by tensile cracking. Thus, the tensile softening, see Sections 3.2.1-3.2.2, was used as a constitutive model for concrete in Abaqus since the brittle behaviour dominates.



Table 3.2 Material properties of C20/25 concrete class used in finite element model.

Density [kg/m³]	2700
Young' s Modulus [GPa]	30
Poisson's ratio [-]	0.2
Tensile strength [MPa]	2.2
Compressive strength [MPa]	28
Fracture Energy [Nm/m ²]	133
Fracture toughness [MPaVm]	0.45

^{*}The fracture toughness was assumed by Sohrabi and Sanchez Loarte (2017).

3.4.3 Interface and boundary conditions

The two-dimensional model consists of two parts of each model, as shown in Figure 3.9. The interface of the two separated parts was modelled by an interaction function to simulate the surface behaviour. A surface-to-surface interaction was made with interaction properties describing cohesive, normal and damage behaviour. A boundary condition with vertical restraint was applied to the bottom surface of the model; see Figure 3.9, while the top part of interaction is free to move in all directions. The analyses were made using a load-control loading system.

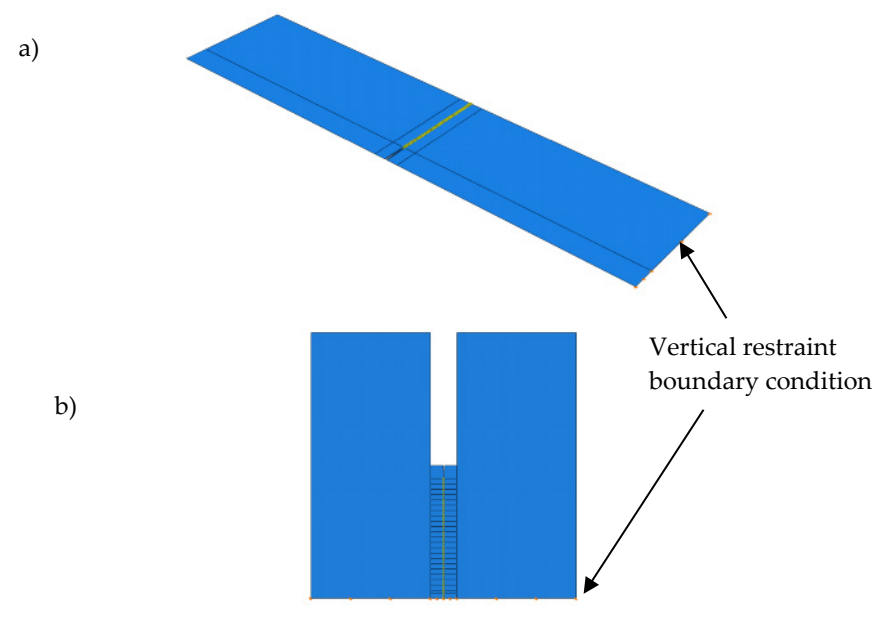


Figure 3.9: Cohesive interaction of a) model 1 and b) model 2, subjected to water pressure at an initial crack.

The FE models were defined with eight-nodded solid elements (CPS4R) with reduced integration. The cohesive interaction model was also defined with eight-nodded with reduced integration (CPS8). The numbers of elements were 11200 with 51533 degrees of freedom.



3.4.4 EF results

Two pressure cases have been investigated; case (a) pressure at the initial crack surface and case (b) pressure along crack propagation, and are presented in Figure 3.10. As mentioned in Section 3.4, case (a) can be approximated as the dynamic force causing sudden crack propagation. While in case (b) water pressure has been fully able to develop a wet surface. In Figure 3.10, for a certain crack propagation distance, the force is significantly higher when the crack has not yet developed a wet surface, whereas the force is less for the crack with the fully developed wet surface.

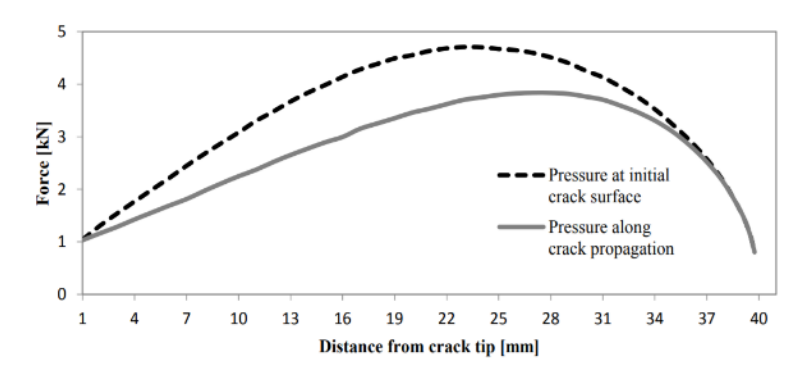


Figure 3.10: Forces for the two pressure conditions of model 1 (Sohrabi and Sanchez Loarte, 2017).

The pressure distribution varies along the crack propagation. As can be seen in Figure 3.11, when a macrocrack is formed, the pressure is developed as evenly distributed and increases slightly in order to continue the propagation. Thereafter, the pressure decreases due to increased fracture area and follows the same pattern along the propagation until reaching total separation of the specimen. It is important also to note that the initial loading conditions have a significant effect on the pressure distribution where for the Model 2, it requires less pressure to initiate the propagation behaviour, by almost a factor 10 compared to Model 1. This is due to the effect of pressure acting at the borehole surface and the high-pressure concentration at the initial crack length. The conclusion of this can be explained as the geometrical size effect of the initial crack.

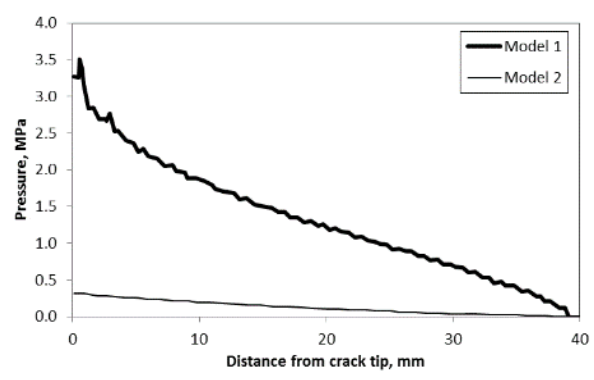


Figure 3.11: Water pressure distribution for each crack extension for Model 1 and 2.



3.5 CONCLUSIONS

In this work, simple finite element models were examined based on the finite element principle with surface-to-surface interaction describing cohesive, normal and damage behaviour. The main conclusion from the numerical examples is that the initial loading conditions have a significant effect on the pressure distribution. Two models were investigated, providing horizontal and vertical initial crack i.e. model 1 and 2, respectively, see Figure 3.9. It was concluded that the initial crack of model 2 requires less pressure to propagate by almost a factor 10 compared to model 1, see Figure 3.11. This is due to the effect of pressure acting at the borehole surface and the high-pressure concentration at the initial crack length. But this is valid only when the water pressure is directly applied on the sides of the boreholes of the specimens.



4 Investigation method

This chapter gives a brief description of the experimental test including the setup, specimen properties, fabrication and procedure. This experimental test was a pilot project where a small sample was tested to investigate the behaviour of an actual dam. The main purpose of the experimental test was to study the propagation influenced by water pressure in concrete cracks. The small specimen was considered to be appropriate to study this phenomenon. The test was performed at the Concrete Structures division at KTH Royal Institute of Technology.

4.1 CONCRETE MIX

Many concrete mixes were tested in order to produce low strength concrete to enable the use of existing equipment. First, according to the received recommendation from the Swedish Cement and Concrete Research Institute, the concrete compositions were designed for low compressive strength (around 6-10 MPa). The mix proportions of the concrete mix are presented in Table 4.1. The obtained compressive strength of the concrete was 20 MPa which is not what expected since the used water/cement (w/c) ratio was 0.7. Another mix was based on a laboratory investigation of macroscopic ice lens growth in hardened concrete according to Rosenqvist et al. (2016), where the mixes were designed with w/c ratio in the range of 0.5 to 1.4. Portland cement was used as a binder. No air entraining agent was used. In this study, the concrete mix with w/c-ratio 1.4 was selected for the experiment where concrete with high w/c-ratio has high porosity and low strength, see Table 4.1. After pre-mixing of cement and aggregate, water was added and mixed for three minutes. The air content was determined. A table vibrator was used to vibrate the concrete in the specimen and the control specimen (cube). The cylindrical specimen and cube are cured at room temperature.

Table 4.1: Concrete mix proportions and compressive strength

Mixture proportions	Swedish Cement and Concrete Research Institute	Rosenqvist et al. (2016)
Cement [kg/m³]	240	150
0 – 8 mm [kg/m³]	1930	1912
w/c-ratio	0.7	1.4
Air content [%]		5
Compressive strength, MPa	20	4.6
Testing age, days	7	10



4.2 FABRICATION OF TEST SPECIMENS

In this study, a concrete cylinder of 100 mm in diameter and 200 mm in length was cast as well as one concrete cube 100×100×100 mm.

4.2.1 First attempt

In this project, two experimental setups were used. A cylinder with a horizontal initial crack was first set up to agree with the FE model that has been developed by Sohrabi and Loarte (2017), see Figure 4.1. Thus, the concrete specimen was designed as a cylinder with a diameter of 100 mm, see Figure 4.2. An anchoring steel flange was installed on the top of the specimen to anchor it to the penetrability meter. The height of the borehole was determined to be half of the specimen's height. This height was long enough to exclude the effect of stress concentration caused by anchoring. In the centre of the specimen, a circularly shaped crack of plastic material was embedded in a tube forming the pressure area. The crack was 60 mm in diameter, extending 10 mm from the borehole.

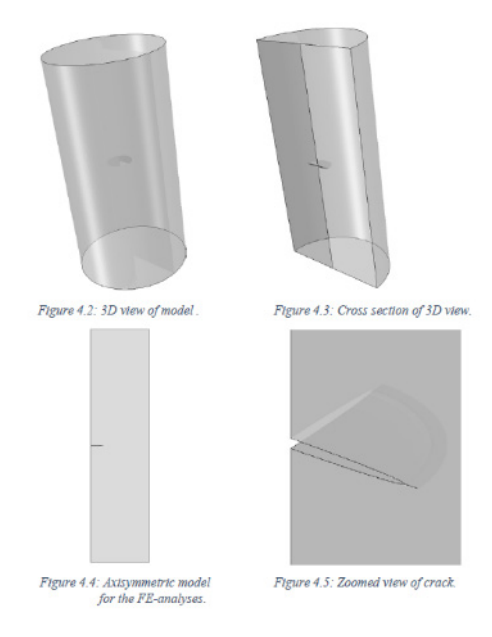


Figure 4.1: Finite element model of master study (Sohrabi and Loarte, 2017)



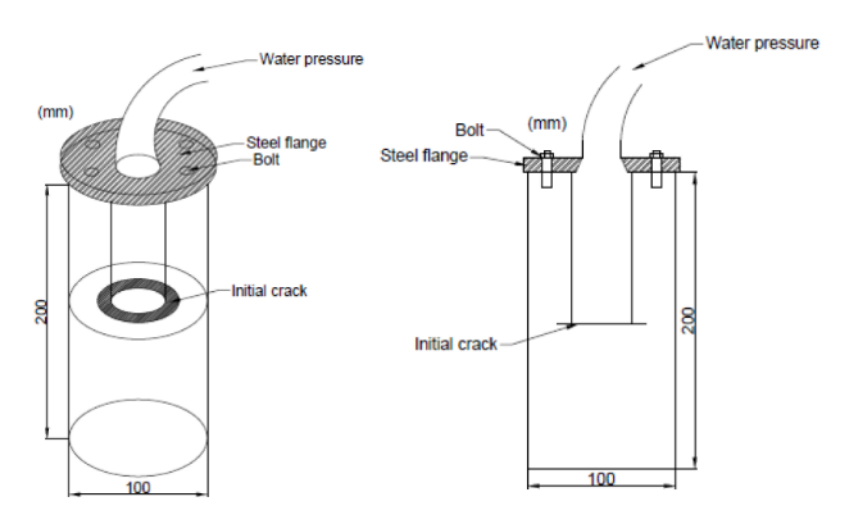


Figure 4.2: Three dimensional and side view of the experimental specimens (Sohrabi and Loarte, 2017)

The concrete was mixed according to a mix of 20 MPa compressive strength, in Table 4.1 and placed into cylinder moulds. In the centre of the specimen, a circularly shaped plastic sheet representing the crack was placed, see Figure 4.3 (a). The size of the tube was determined in accordance with the holes of the steel flange. To avoid any leakage of water, the hole was made a few millimetres larger than the holes of the flange. A tube of aluminium was placed in the middle of the crack surface and the remaining concrete was added. The plastic sheet was embedded in oil to avoid any friction during the removal. The concrete was under hardening in four hours before the removal of the embedded crack and tube. Vibration on the upper part of the specimen was not possible due to the embedded crack and tube that would have been moved and sealed with the cement paste. This resulted in uneven surfaces and incompact concrete, see Figure 4.3 (b and c). It was decided, in order to have an even surface that the three specimens were sawn to the height of the crack plane and a new borehole with a small height (maximum 30 mm) was drilled. An adapter, see Figure 4.4 (a), was connected to the specimen with adhesive glue, e.g. plastic padding. Horizontal crack is hard to create after hardening; hence vertical crack had to be added. The vertical crack was created with a drill machine.



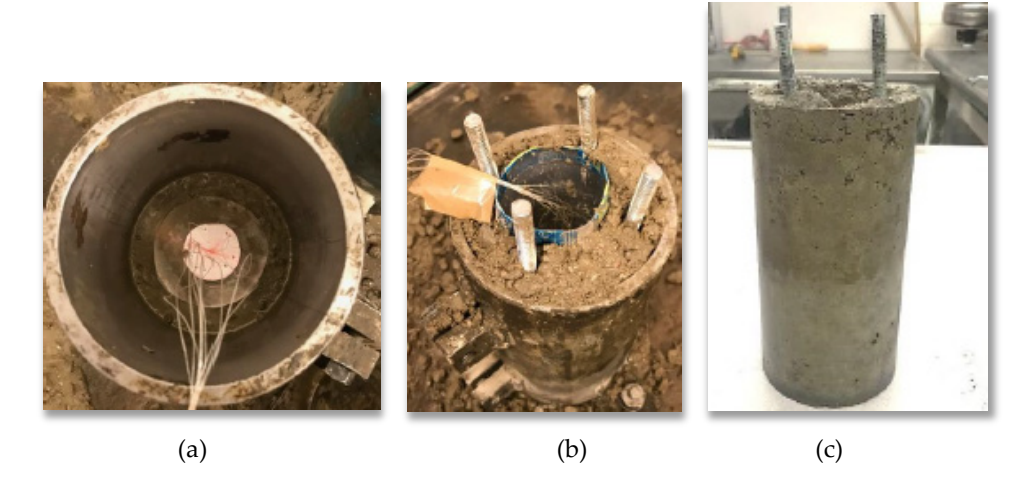


Figure 4.3: Specimen: (a) embedded crack, (b) tube and (c) specimen after casting

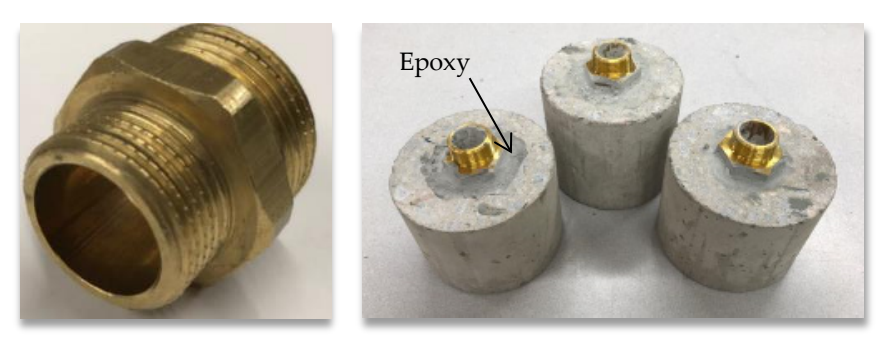


Figure 4.4: Photo of (a) the adaptor and (b) adaptor glued to the concrete specimens

The modified specimen resembles the specimen used by Slowik and Saouma (2000), see Figure 4.6, with some changes in the geometry to use the available forms in the laboratory.

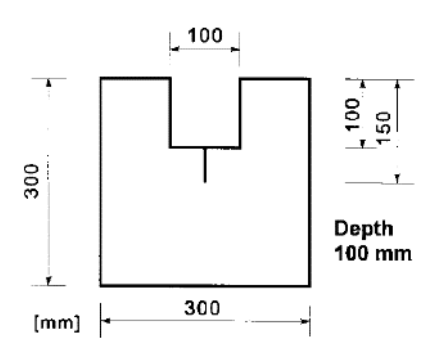


Figure 4.6: Cube specimen dimensions of Slowik and Saouma (2000).

4.2.2 Second attempt

Since the concrete strength was higher than what was desirable a second attempt was performed using the mix properties of Rosenqvist et al. (2016), see Table 4.1. Moreover, for some practical reasons the results from the first attempt were



unexpected, as will be described in Chapter 5, a new proposed setup was performed according to the recommendations from Professor Anders Ansell (Concrete Structures division at KTH).

In this attempt, a steel frame basically consisting of a steel water pipe of 3.5 cm was designed and embedded in concrete to distribute the water vertically in one direction, see Figure 4.6. Three steel rings were welded, two along the water pipe to provide a good bond between the water pipe and the surrounding concrete and one at the end of the pipe, see Figure 4.6(a). The frame was fixed to the cylindrical mould to reduce the probability of the movement of the embedded pipe inside the concrete during the casting, see Figure 4.6(b). At the end of the pipe, a circular steel plate was fixed. The plate was mounted underneath the last rings by using a steel wire passing through a water pipe.

Proper compaction of concrete while casting specimens was essential to achieve a better and more consistent mixture. The concrete was vibrated using vibration table for 8 sec, see Figure 4.6(c). Then the specimens were cured at room temperature for 10 days.



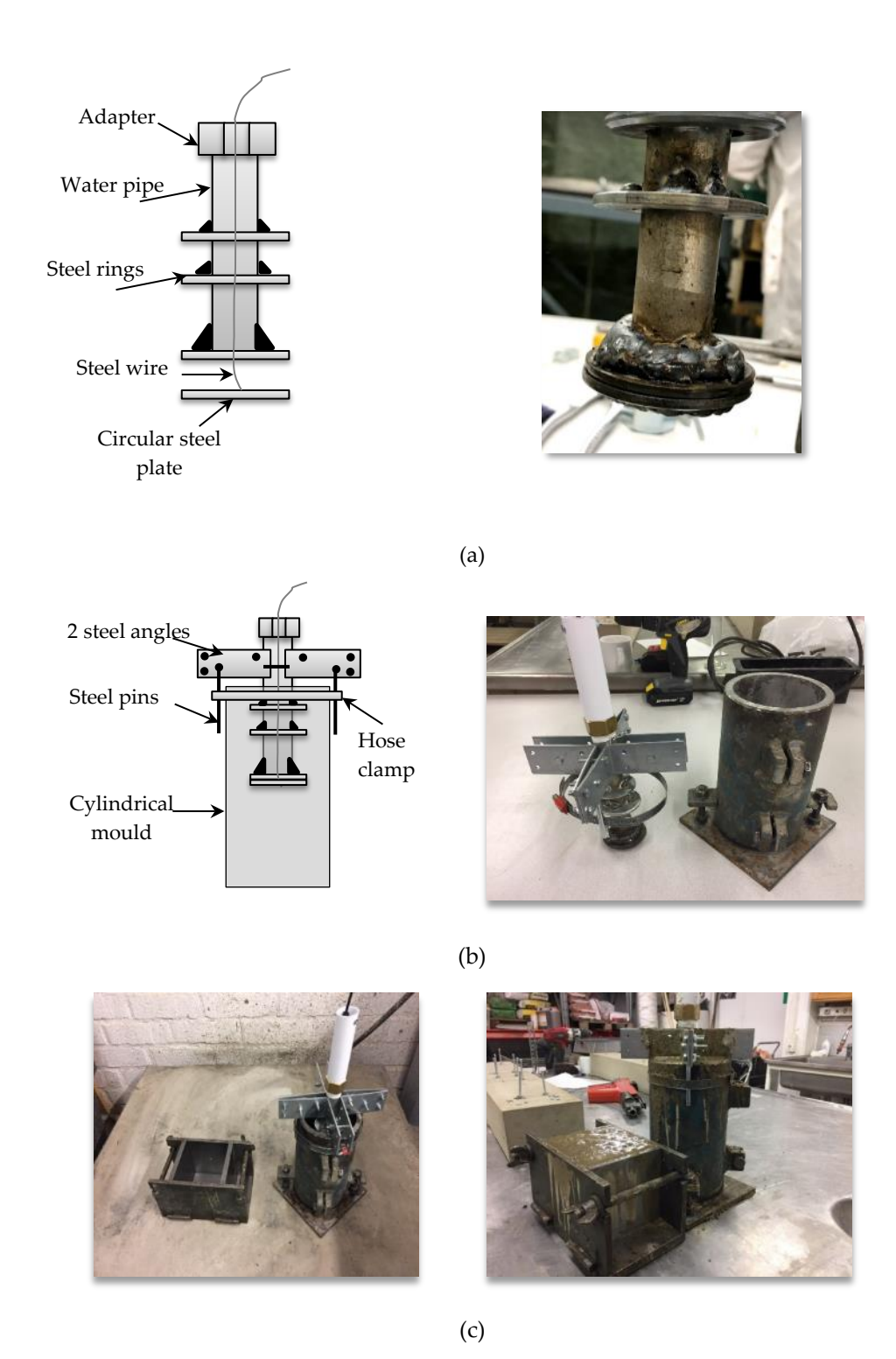


Figure 4.6: Second attempt setup (a) a steel frame (b) fixing steel frame inside the mould and (c) casting concrete

4.3 EXPERIMENTAL PROCEDURE

4.3.1 Applying water pressure

For the two attempts, the specimen was connected to penetrability meter by a system of adapters and a valve, see Figure 4.7. A sensor was connected to this valve to measure the applied water pressure, see Figure 4.8. The measuring capacity of the sensor was up to 20 bar. A constant load of water pressure was applied to the specimen through the connected hoses, see Figure 4.8. The applied pressure was supplied by the gas container and the pressure was controlled by a pressure regulator. The water flew from the grout tank which was filled with water. The pressure capacity of the grout tank was up to 20 bar also. The pressures were successively increased by the pressure regulator. The test was performed under quasi-static loading and the load was kept constant for at least 5 min period of time. In this experiment, the applied water pressure was up to 20 bar within almost 90 min. Although, the gas container with 300 bars capacity, the applied pressure was restricted to 20 bar since the capacity of the sensor and grout tank was up to 20 bar.

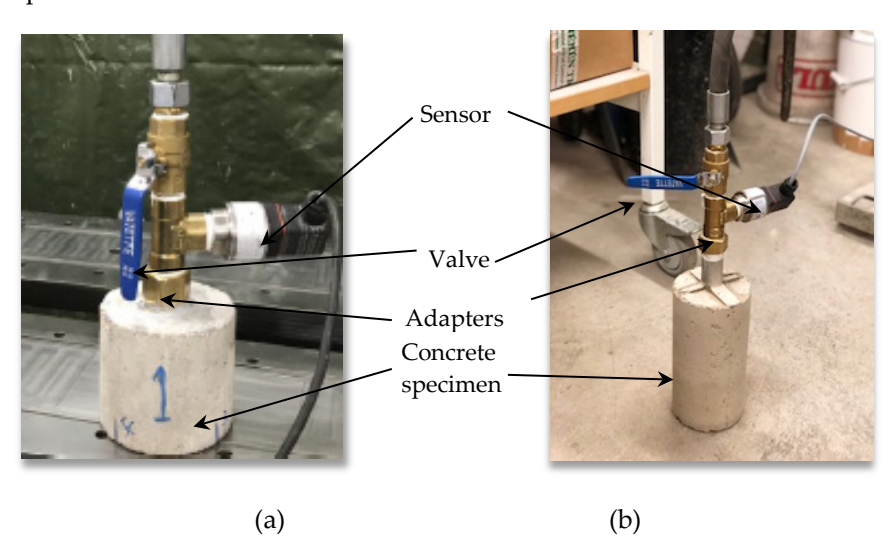


Figure 4.7: Concrete specimens with adapters, (a) first and (b) second attempts.

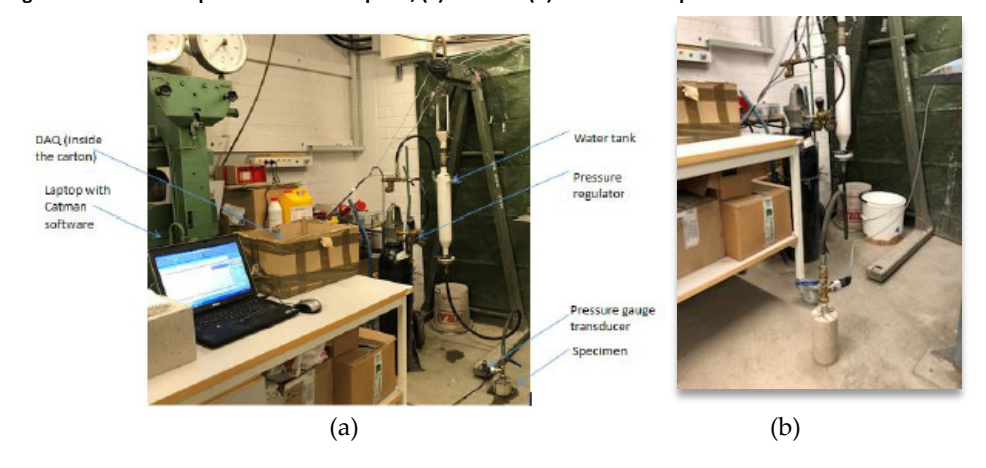


Figure 4.8: Applying pressure, (a) first attempt specimen, permeability meter and computer (b) the concrete specimens connected to the permeability meter in the second attempt.



4.3.2 CT scan

As mentioned in Section 2.2, in this study, a KTH X5000-CTX-ray CT scanner was used to obtain the detailed microscopic structure of the concrete core samples for further visualization and characterization. The X5000 CT scanner is a seven-axis universal x-ray imaging system designed for the inspection of large objects; it can accommodate a variety of part shapes, sizes and weights. It has two energy sources: 225 kV with micro focus and 450kV.

The x-ray scanning process includes sample preparation, warming- up the scanner, pre-scan settings, scanning, detector calibration and CT calibration. A concrete specimen was placed on the turntable between the X-ray source and the detector. An X-ray beam transmitted through the specimen while the turntable completed a full rotation at a constant speed. The digital images captured by X-ray CT are two-dimensional images.

Beam hardening artifact is manifested in CT images with brighter edges than the centre of the image. Beam hardening artifact reduces the quality of the scanned image and hence affects the results. This artifact can be corrected using digital image processing techniques.

The CT work done in this project can be divided into two sections as follows:

- Visualization of water in concrete samples.
- A drilled steel fibre concrete core was partially submerged in 50 mm water level for 2 weeks and then scanned.
- Visualization of cracks in concrete induced by pressurized water.
- Samples prepared and conditioned as explained in Section 4.3.1 were scanned immediately after their conditioning for crack initiation and propagation.

The design of a rotational system to apply controlled water pressure on a concrete sample, while scanning the sample was also evaluated; however, due to cost and time resources, it was not suitable. In addition, the required synchronization with the rotational scanning table, as well as concerns about the safety/integrity of the CT equipment were also major issues. Therefore it was decided to run the pressurized water test in the concrete lab, and immediately after scan the sample. In addition, since no cracking was induced during the pressurized water test, there was no need to try to scan the concrete sample while applying pressurized water.



5 Results and discussion

In this chapter, the results of experiment test are presented. In the first section, the applied water pressure is presented for the two attempts. As mention in Section 2.2, CT imaging has been used to detect the crack propagation. In the later section, a visualization of the concrete specimens before and after the test is presented.

5.1 WATER PRESSURE TIME HISTORY

A successively increasing load was applied to the specimens. After applying the specific water pressure, the valve closed to control if the load remained constant or if leakage occurred. The pressure was kept constant for a while in order to let the cracks propagate.

5.1.1 First attempt

Three specimens were prepared and tested. Figure 5.1 shows the water pressure time history for specimen 1, 2 and 3. In Figure 5.1 and for specimen 1 the pressure was increased to a level of 0.27 MPa before closing the valve and letting the pressure be constant. After 2 minutes, the pressure decreased although the applied water pressure was constant. After 40 minutes, the pressure decreased to zero. For specimen 2, see Figure 5.1, the water pressure was increased to 0.23 MPa before closing the valve. The pressure remained constant for almost 1.3 minutes before then the water pressure decreased. It can be seen from Figure 5.1 that the pressure decreased in specimen 2 faster than in specimen 1 and reached a low-pressure level after just a few minutes. For the later test of specimen 3 the water pressure was increased to level 0.21 MPa, see Figure 5.1, and the water pressure remained constant and the pressure was manually increased further to 0.27 MPa after almost 27 minutes. Then, the pressure was increased to 0.4 MPa after 5 minutes. The pressure remained constant for almost one minute then decreased to 0.17 MPa. Attempts to reach a higher level of pressure were performed as in Figure 5.1. The last increment of the pressure was up to 0.72 MPa and still, no fracture in the specimen 3 occurred. After 70 minutes, the water pressure decreased to almost 0.17 MPa and then it was decided to finish the test.



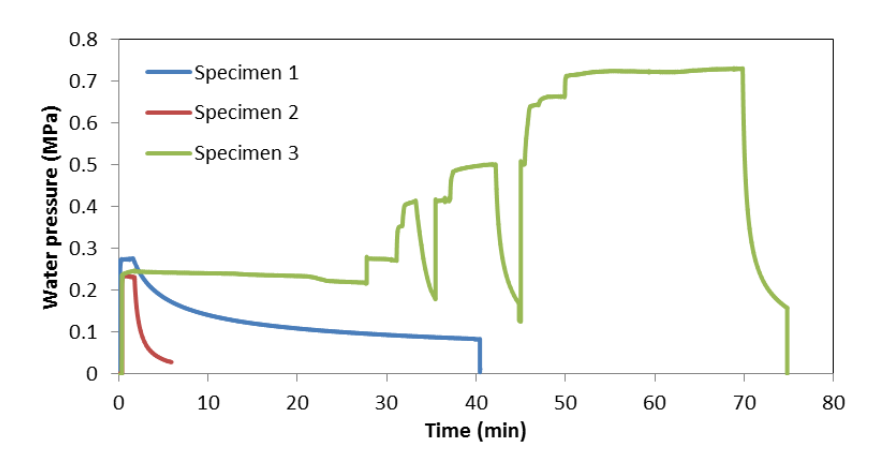


Figure 5.1: Water pressure time-history for three specimens of the first attempt.

It can be concluded from Figure 5.1 that the sudden decrease of water pressure might be due to bond failure between the epoxy in the boreholes and the concrete surface, see Figure 4.4 (b). The bond failure caused a possibility of leakage and the water pressure decreased although the applied pressure from the penetrability meter was constant. This happened quite early in specimen 1 and 2, at 2 and 1.3 minutes, respectively. For specimen 3, the water pressure was constant for the first increment of 0.25 MPa. At water pressure level 0.41 MPa, leakage occurred and the pressure decreased and prevented the continuation of the test.

5.1.2 Second attempt

The second setup was investigated and the specimen connected to penetrability meter. The water-pressure time history is presented in Figure 5.2. In this setup, the water pressure was increased at almost regular intervals by applying 0.2 MPa every 5 minutes. It can be seen that no leakage occurred and the test was terminated up to 19 bars (0.19 MPa) which is the maximum capacity that can be used in this device setup. Figure 5.3 shows some photographs of the specimens during the testing. The first drop has been seen after almost 20 minutes from the starting time of the test.

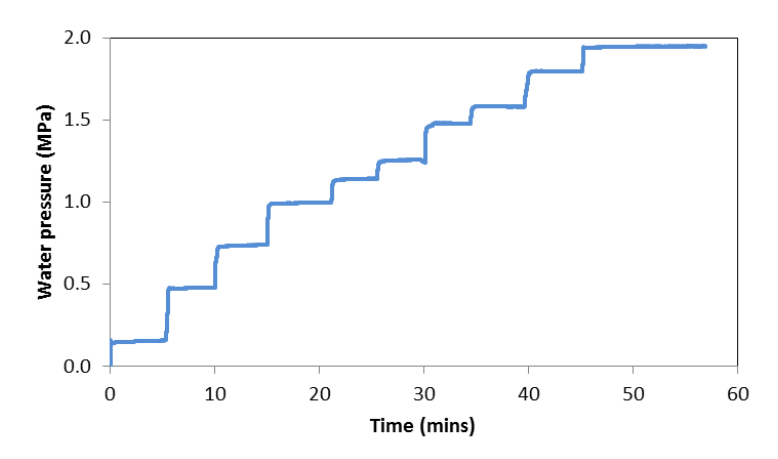


Figure 5.2 Water pressure time-history of the second attempt.



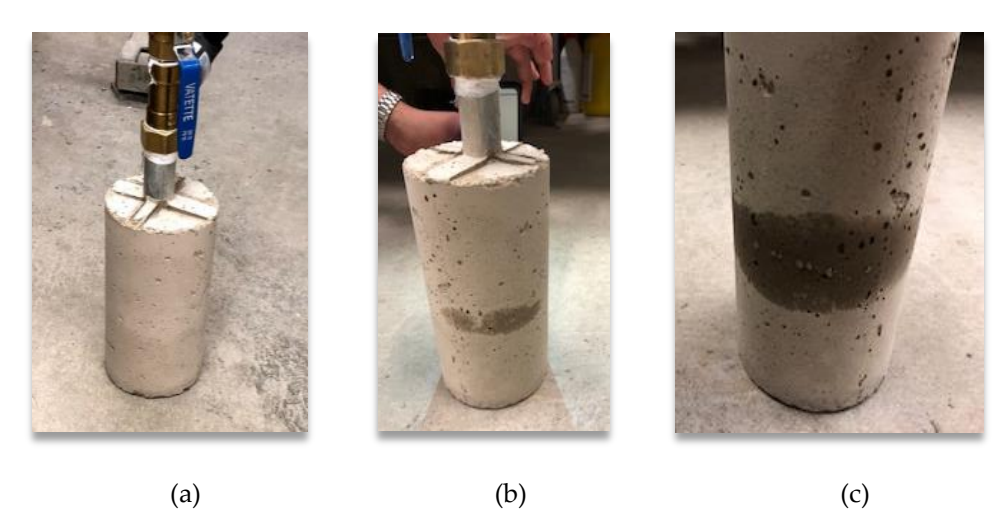


Figure 5.3: Photographs of the specimen during the testing time, (a) during the first 5 minutes, (b) after 10 minutes and (c) first drop after 20 minutes.

As mentioned in Section 3.2, the crack initiates when the concrete tensile stress exceeds its tensile strength and in order to understand the effective pressure from the penetrability meter, a small calculation has been made to investigate that the applied pressure was higher than the tensile strength of this type of concrete.

The developments of tensile and compressive strengths are closely related, but there is no documented definite relationship between these two types of strengths, so several relations have been proposed, see (Oluokun, 1991 and Nihal Aruoglu and Ergin Aruoglu, 2006). Suggested relationships between compressive (f_{cc}) and strength tensile (f_{tc}) that include concrete at early ages, from the first 6 h after placement of concrete and up to maturity (at 28 days), are presented by Francis A. Oluokun and J. Harold Deatherage (1991). From the properties of the regression lines of their experimental results, it was determined that the tensile strength is proportional to the 0.79 power of the cylinder compressive strength at all ages (up to 28 days) except at the ages of 6 h, or for f_{cc} less than 6.8 MPa when the power was found to be 0.60, as in the following:

$$f_{tc} = 0.127 (f_{cc})^{0.60} \text{ for } f_{cc} < 6.8 \text{ MPa}$$
 (3)

and:

$$f_{tc} = 0.206 (f_{cc})^{0.79} \text{ for } f_{cc} > 6.8 \text{ MPa}$$
 (4)

It should be noted that the above equations show a discontinuity with respect to compressive strength range so that Equation (3) gives a conservative estimation of compressive strength less than 6.8 MPa. This might reflect the uncertainty in the behaviour of concrete at an early age.

However, the compressive strength of cylinder is approximated using the relation between cylinder and cube strength ($f_{cc,cube}$) that is given in (Eurocode 2, 2011), as $f_{cc} = 0.8 f_{cc,cube}$.

Based on the tested compressive strength of concrete in Table 4.1, where the cube compressive strength is 4.6 MPa and by using Equation (3), the tensile strength is



$$f_{tc} = 0.127 (f_{cc})^{0.60} = 0.127 (0.8 \times 4.6)^{0.60} = 0.277 \text{ MPa}$$

The water flows through the water pipe and is spread from the adjacent plates; see Figure 5.4. Thus, the water pressure at the tip of these adjacent plates (P_t) must be higher than 0.277 MPa to initiate a crack in the concrete. Calculations have been done to find P_t . The test was terminated at 0.19 MPa for safety considerations. Then, P_t can be calculated as:

 P_t = (water pressure in water pipe × area of water pipe) / (area of circular plate)

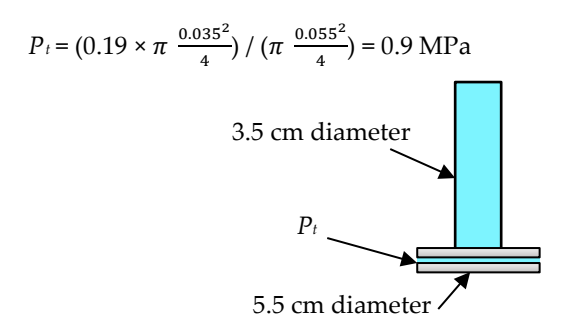


Figure 5.4: Configuration of the test set up.

Then, the applied water pressure for the second attempt was 0.9 MPa which was higher than the estimated tensile strength i.e. 0.277 MPa. It was expected that an initial crack would occur but the concrete absorbed the water and damped the effect of water pressure, therefore, no local damage happened at the tip of adjacent plates and the test was terminated.

5.2 TOMOGRAPHY VISUALIZATION

In this section, an additional tomography study is summarized. The aim was to investigate if it is possible to visualize the water penetration into the crack. The specimens used in the previous section are cast in the laboratory. In contrast to these specimens, which were cast individually, the specimen used in Section 5.2.1 is extracted from a single shotcrete beam using a coring drill.

5.2.1 Visualization of water in concrete sample

In order to obtain information on the possibility to observe differences in water saturated and dry concrete using tomography, a drilled steel fibre concrete cylinder of size 125 mm in diameter and 50 mm in length, was partially submerged in 50 mm water level for 2 weeks, see Figure 5.5. Then the specimen was scanned using X-ray DR (Digital Radiography), see Figure 5.6. It can be seen from Figure 5.6 (a) that the sample was scanned when it was submerged in water while in Figure 5.6 (b) the sample was removed from the water and scanned. From the obtained X-ray images in Figure 5.6, it can be seen that it was not possible to differentiate between dry and wet concrete.



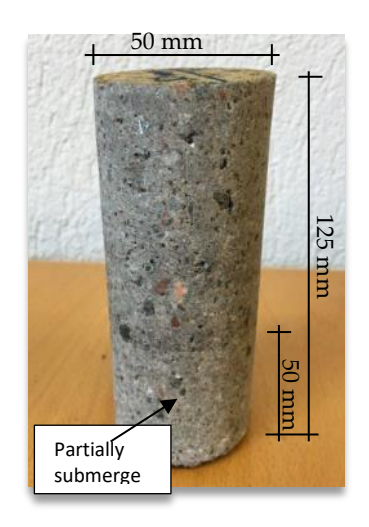


Figure 5.5: Steel fibre concrete sample.

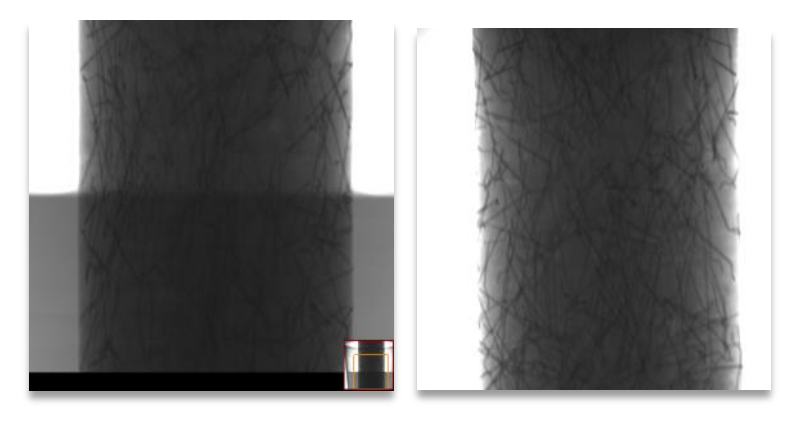


Figure 5.6: X-ray images (a) sample submerged in the water and (b) sample after removing from the water.

5.2.2 Visualization of cracks in concrete induced by pressurized water

First attempt

Since leakage occurred quite early in specimens 1 and 2, only specimen 3 was of interest to inspect in the tomography. The specimen after the hydraulic testing can be seen in Figure 5.7. After the application of pressurized water, no changes were detected around the initial crack.



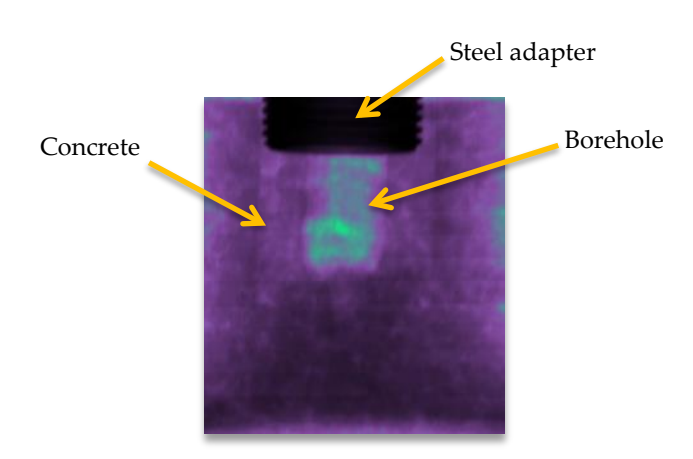


Figure 5.7: 2D visualization for specimen 3 after hydraulic testing.

Second attempt

For the second stage of this study, a comprehensive 3D X-ray CT evaluation was completed. As mention in Section 2.2, the X-ray CT system is an in-house built system which consists of an X-ray source, a rotating turntable to hold the specimen, and an image intensifier detector. The X-ray beam is modulated into a cone type beam by using a collimator. The CT images used in this study were obtained with the energy source of 225 kV without beam filtration, see Figure 5.8. The scanning resolution is $1645 \times 1960 \times 1625$ voxels with voxel size $65.81 \times 65.81 \times 65.81$ microns.



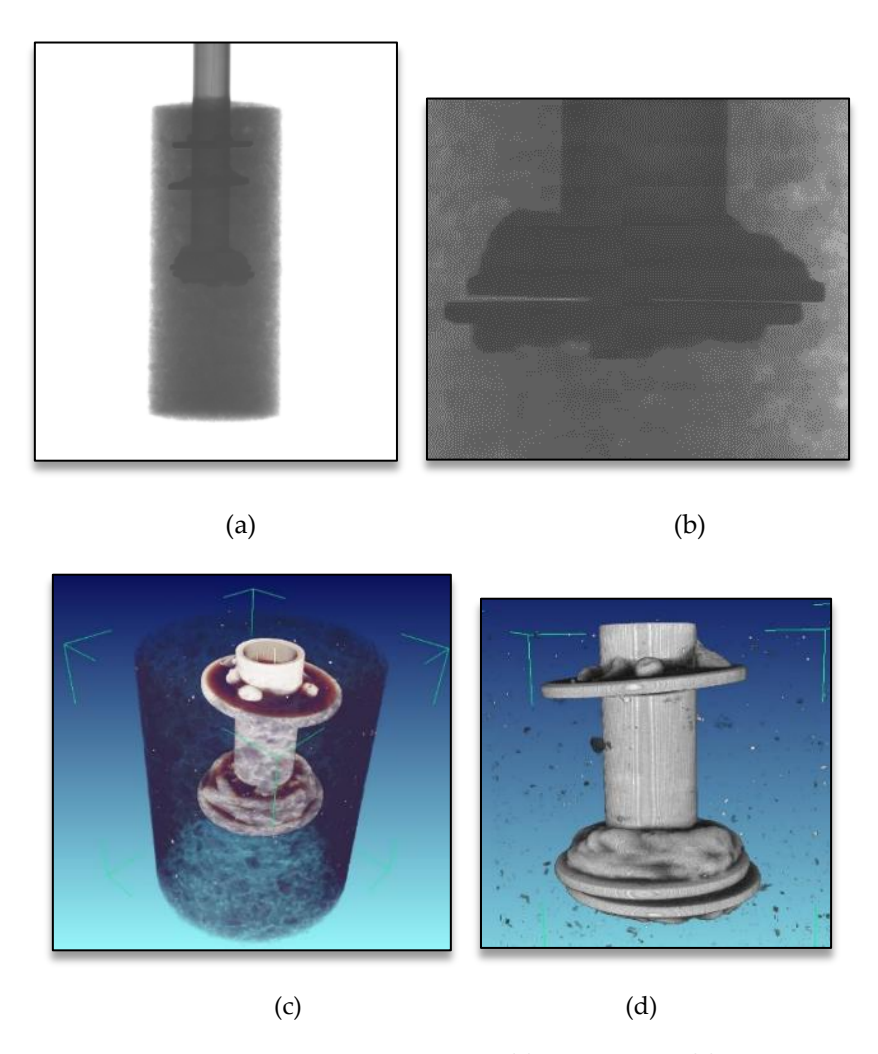


Figure 5.8: 3D Visualization of the concrete sample, X-Ray scan (a) entire specimen, (b) local view of two steel plates, and 3D X-ray CT scan (c) entire specimen, (d) extracted steel pipe of the specimen.

A typical original two-dimensional CT image from the concrete specimen is shown in Figure 5.9. Each image, gathered in this test, has 1090 × 1090 pixels. A total of 1981 images were taken at intervals of 0.067 mm. The CT image, shown in Figure 5.9, consists of 255 levels of intensity that correspond to different densities within a specimen. The brighter colour represents a higher density material, whereas the darker colour represents a lower density material. Then, it can be realized to distinguish the four compositions, i.e. steel pipe, air void, cement and aggregate in a concrete mixture where the dark spots in the image indicate air-voids and bright regions denote the steel pipe while the grey regions denote the concrete-matrix i.e. cement and aggregate. With the visualizing system, reconstructed images of these two-dimensional CT images are converted into a three-dimensional image to quantify the internal structure of concrete specimens, as shown in Figure 5.8 (c) and (d). The four volumetric compositions can be identified separately according to the measured grey levels that correspond to different densities within the specimen, i.e. segmentation process. For example, Figure 5.8 (d) shows the steel pipe in the concrete specimen.

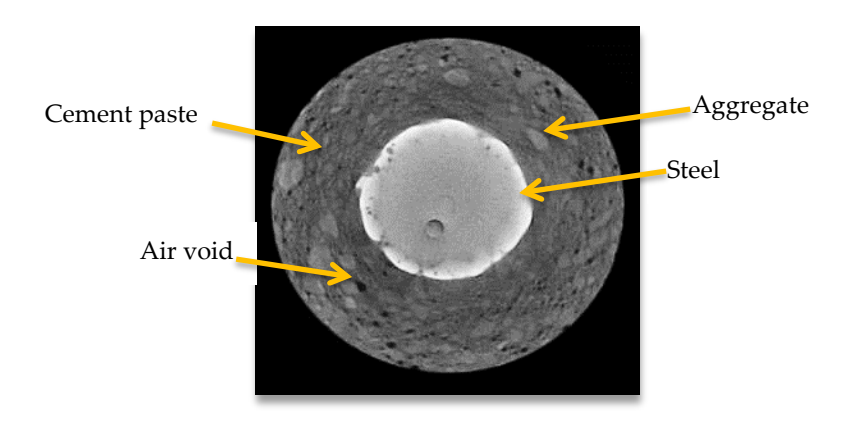


Figure 5.9: CT image of the concrete cylinder of 100 mm diameter.

Despite using 3D X-ray CT; it was not possible to distinguish between dry and wet sections of the concrete under the experimental setup, sample sizes, and algorithms utilized in this project. Hence, further investigation is required on this subject.

As mentioned in Section 2.2, KTH Materials Laboratory has successfully used 3D X-ray CT for crack detection on concrete; unfortunately, no cracking was induced on the concrete specimen by the pressurized water designed and implemented for this project despite the applied pressure was 1.9 MPa which is higher than the estimated tensile strength of the used concrete for the second attempt.

5.3 DISCUSSION

The examples reported in Chapters 4 show that the technology and equipment have great potential for future work on crack propagation, however, sample design and preparation, as well as testing need further development.

The test setup included two design attempts, with and without the embedded pipe. In the first attempt, three specimens were defined similarly with some minor differences in dimensions; the loading results differed for each of those. Leakage occurred fastest in specimen 2 and slowest in specimen 3, see Figure 5.1. The reason for the leakage is believed to be poor bonding between the sealing epoxy padding and the adapter. A reason for this can be that the used concrete strength was higher than expected.

In the second attempt, the setup was more promising since the water with high pressure flew through the embedded pipe and the water spread from two plates to the concrete. Due to safety reasons, the load could not be increased to more than 1.9 MPa. According to the simple calculation in Section 5.1 second attempt, the applied water pressure was 0.9 MPa which was higher than the estimated tensile strength of 0.277 MPa. It was expected that an initial crack would occur but the concrete absorbed the water and damped the effect of water pressure, therefore, no local damage happened at the tip of adjacent plates and the test was terminated. Another reason could be that the pipe was partially filled with cement paste then the applied water pressure might be lower than the calculated value.



6 Conclusions and further research

The project has been interdisciplinary, combining finite element modelling and experimental work to study crack propagation due to water pressure. The experimental part aimed at investigating the possibilities for conducting a test to study crack propagation due to water pressure. Two trial setups have been dimensioned to conduct pilot trials to evaluate the test methodology. In the following, the main conclusions and recommendations are given, regarding tomography and testing techniques.

6.1 CONCLUSIONS

The main conclusions are given, regarding tomography and testing techniques:

- The examples reported in this work show that the technology and equipment have great potential for future work on crack propagation, however, sample design and preparation, as well as testing need further development.
- 2. Under the experimental setup, sample sizes, and algorithms utilized in the 3D X-ray CT evaluation; it was not possible to visualize water in the concrete.
- 3. Due to cost and time resources, it was not possible to design an experimental setup to allow the application of pressurized water to a concrete sample while scanning it. The required synchronization with the rotational scanning table, as well as concerns about the safety/integrity of the CT equipment were also major issues.
- 4. The penetrability meter can be used to apply water pressure. This device is available at KTH Royal Institute of Technology. The pressure is controlled by a pressure regulator. For practical reasons, the experiments are performed only with a 20 bar pressure which is equal to 2 MPa.
- 5. The embedded pipe in the concrete specimens that was fixed to mould before the casting reduces the inconsistency of the concrete specimens. In other words, it would have been possible to vibrate the specimen during the casting of concrete specimens.
- 6. Hazards exist in applying the high water pressure. There is a need to control the specimens that are in place under high water pressure to eliminate potential safety hazards when the specimen reaches the point of explosion.

6.2 RECOMMENDATIONS

Based on the previous experience with the tested specimens of concrete, some items to be taken into account in the continued setup development could be identified as a further work. The main recommendations are presented:

- 1. Low compressive strength concrete should be used to facilitate crack initiation during applying water pressure.
- 2. The possibility of applying gas instead of water using the penetrability meter should be explored.
- 3. Further investigation is needed for detection of water in concrete when using the CT system.



4. It is partly about the steel plates that should be ground so that they are tightly seated against each other and no cement paste can come in between them by using magnets. The magnets should be so strong that they just clamp the steel plates while concrete casting. The magnets can be replaced by electromagnets that can be disconnected when the concrete has cured, see Figure 6.1. A soft layer should be also placed underneath the two plates that the lower plate could easily separate during applying water pressure.

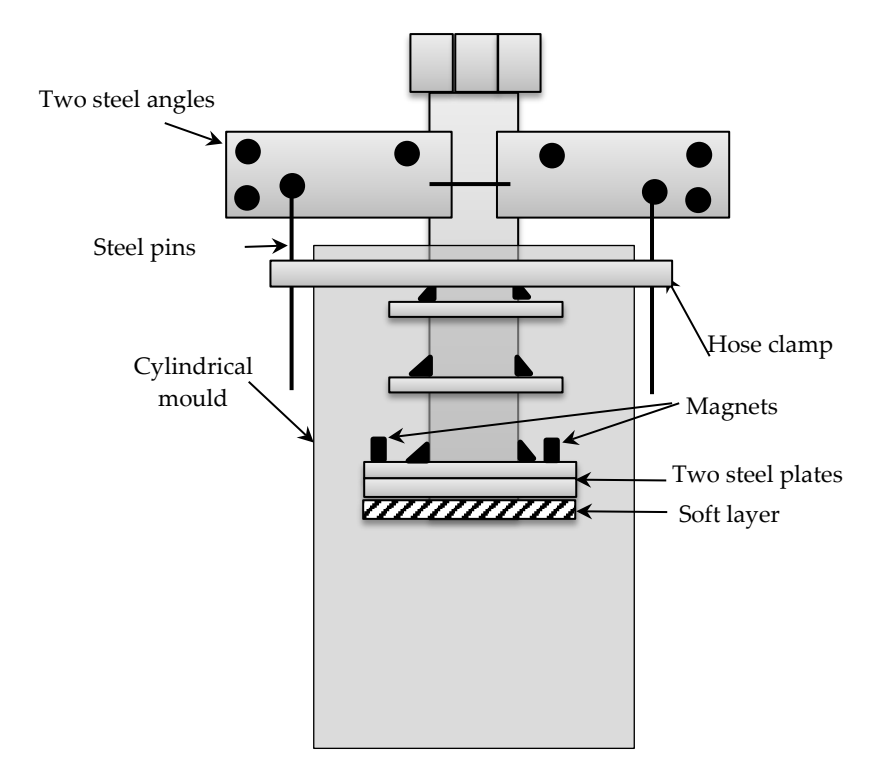


Figure 6.1: Suggested modified setup.

References

Ansell, A., Ahmed, L. and Guarin, A. (2017) 'Computed tomography as investigation method for steel fibre reinforced tunnel shotcrete', in *XXIII Concrete Research Symposium*. Aalborg.

Björnström, J., Ekström, T. and Hassanzadeh, M. (2006) *Dammsäkerhet :spruckna betongdammar : översikt och Elforsk, beräkningsmetoder.*

Bruhwiler, E. and Saouma, V. (1995) 'Water Fracture Interaction in Concrete--Part II: Hydrostatic Pressure in Cracks', *ACI Materials Journal*, 92(4). doi: 10.14359/973.

Dassault Systémes, 2014. ABAQUS 6.14 Documentation

Durable Concrete Structures: Design Guide (1992). Thomas Telford Publishing. doi: doi:10.1680/dcs.35492.

Eurocode 2 (2011) *Design of concrete structures - Part1-1: General rules and rules for buildings.* CEN, Brussels, EN 1992-1-1.

Farrokh, J., Pierre, L. and René, T. (2005) 'Seismic Water Pressure in Cracked Concrete Gravity Dams: Experimental Study and Theoretical Modeling', *Journal of Structural Engineering*. American Society of Civil Engineers, 131(1), pp. 139–150. doi: 10.1061/(ASCE)0733-9445(2005)131:1(139).

Francis A. Oluokun and J. Harold Deatherage, E. G. B. (1991) 'Splitting Tensile Strength and Compressive Strength Relationships at Early Ages', *Materials Journal*, 88(2). doi: 10.14359/1859.

Hansen, K. D. and Roehm, L. H. (1979) 'The response of concrete dams to earthquakes', *Water Power Dam Construction*, 4 II).

Hassanzadeh, M. and Westberg, M. (2016) *Inventering av spricktyper I vattenkraftens betongkonstruktioner*.

Hillerborg, A., Modéer, M. and Petersson, P.-E. (1976) 'Analysis of crack formation and crack growth in concrete by means of fracture mechanics and finite elements', *Cement and Concrete Research*. Pergamon, 6(6), pp. 773–781. doi: 10.1016/0008-8846(76)90007-7.

Ketcham, R. A. and Carlson, W. D. (2001) 'Acquisition, optimization and interpretation of X-ray computed tomographic imagery: applications to the geosciences', *Computers & Geosciences*. Pergamon, 27(4), pp. 381–400. doi: 10.1016/S0098-3004(00)00116-3.

Malm, R. (2016) Guideline for FE analyses of concrete dams.

Nejad Ghafar, A. (2017) An Experimental Study to Measure Grout Penetrability, Improve the Grout Spread, and Evaluate the Real Time Grouting Control Theory, TRITA-JOB PHD NV - 1027. KTH Royal Institute of Technology. Available at: http://kth.diva-portal.org/smash/get/diva2:1158297/FULLTEXT01.pdf.

Nihal Arıoglu and Ergin Arıoglu, Z. C. G. (2006) 'Evaluation of Ratio between



Splitting Tensile Strength and Compressive Strength for Concretes up to 120 MPa and its Application in Strength Criterion', *Materials Journal*, 103(1). doi: 10.14359/15123.

North Star Imaging Ins (2016) *X5000 system*. Available at: http://4nsi.com/systems/x5000/.

Oluokun, F. (1991) 'Prediction of Concrete Tensile Strength from its Compressive Strength: an Evaluation of Existing Relations for Normal Weight Concrete', *Materials Journal*, 88(3). doi: 10.14359/1942.

Rossmanith, H.-P. (1993) 'Fracture and damage of concrete and rock: FDCR-2: proceedings of the Second International Conference on Fracture and Damage of Concrete and Rock, Vienna, Austria, 9-13 November 1992'. Edited by H.-P. (Hans-P. Rossmanith. London: London.

Sha, S. and Zhang, G. (2017) 'Modeling of Hydraulic Fracture of Concrete Gravity Dams by Stress-Seepage-Damage Coupling Model', *Research article at the Department of Hydraulic Engineering*, 2017(Tsinghua University, Beijing).

Slowik, V. and Saouma, V. E. (2000) 'Water Pressure in Propagating Concrete Cracks', *Journal of Structural Engineering*. American Society of Civil Engineers, 126(2), pp. 235–242. doi: 10.1061/(ASCE)0733-9445(2000)126:2(235).

Sohrabi, M. and Sanchez Loarte, J. (2017) *Crack propagation in concrete dams driven by internal water pressure, TRITA-BKN-Examensarbete NV - 522*. Available at: http://kth.diva-portal.org/smash/get/diva2:1130217/FULLTEXT01.pdf.

Wang, Y. and Jia, J. (2017) 'Experimental study on the influence of hydraulic fracturing on high concrete gravity dams', *Engineering Structures*. Elsevier, 132, pp. 508–517. doi: 10.1016/J.ENGSTRUCT.2016.11.046.



CRACK PROPAGATION UNDER WATER PRESSURE

Cracks in concrete structures such as a concrete dam can be exposed to water pressure, for example, uplift pressure. The water pressure can be significant and may result in cracks propagating through the structures and thus it may result in reduced service life.

However, the knowledge of water pressure within the cracks is relatively limited and is often neglected or just roughly estimated. This study aims at investigating how to design an experimental model to evaluate the crack propagation behaviour under the influence of water pressure and how tomography can be used to visualize the crack propagation.

The aim is to get a description of the possibilities and constraints of this combined technology areas as well as the workflow, and thus indirect working time, to use the method of calculating fracture opening along the crack path suitably. Knowledge about the water pressure inside the cracks and interfaces is important for a safer design of hydraulic structures.

Energiforsk is the Swedish Energy Research Centre – an industrially owned body dedicated to meeting the common energy challenges faced by industries, authorities and society. Our vision is to be hub of Swedish energy research and our mission is to make the world of energy smarter!

